A Caveolin Dominant Negative Mutant Associates with Lipid Bodies and Induces Intracellular Cholesterol Imbalance✪

Albert Pol,* Robert Luetterforst,* Margaret Lindsay,* Sanna Heino,‡ Elina Ikonen,‡ and Robert G. Parton*

*Institute for Molecular Bioscience, Centre for Microscopy and Microanalysis and Department of Physiology and Pharmacology, University of Queensland, Queensland 4072, Australia; and ‡Department of Biochemistry, National Public Health Institute, 00300 Helsinki, Finland

Abstract. Recent studies have indicated a role for caveolin in regulating cholesterol-dependent signaling events. In the present study we have analyzed the role of caveolins in intracellular cholesterol cycling using a dominant negative caveolin mutant. The mutant caveolin protein, cav-3^{DGV}, specifically associates with the membrane surrounding large lipid droplets. These structures contain neutral lipids, and are accessed by caveolin 1–3 upon overexpression. Fluorescence, electron, and video microscopy observations are consistent with formation of the membrane-enclosed lipid rich structures by maturation of subdomains of the ER. The caveolin mutant causes the intracellular accumulation of free cholesterol (FC) in late endosomes, a decrease in surface cholesterol and a decrease in cholesterol efflux and synthesis. The amphiphile U18666A acts synergistically with cav^{DGV} to increase intracellular accumulation of FC. Incubation of cells with oleic acid induces a significant accumulation of full-length caveolins in the enlarged lipid droplets. We conclude that caveolin can associate with the membrane surrounding lipid droplets and is a key component involved in intracellular cholesterol balance and lipid transport in fibroblasts.

Key words: caveolin • caveolae • cholesterol • lipid droplets • endoplasmic reticulum

Introduction

Traditionally, caveolae have been defined morphologically as bulb-shaped structures on the cell surface, and biochemically as cholesterol- and caveolin-rich domains (for a recent review see Kurzchalia and Parton, 1999). Over the last few years, it has become evident that the link between caveolins and cholesterol is not restricted to the simple spatial colocalization in liquid-ordered phases on the plasma membrane. Caveolins regulate the intracellular transport of cholesterol in a complex process involving caveolae, the ER, and the Golgi complex (Smart et al., 1996; Scheiffele et al., 1998). Whereas plasma membrane caveolae are the final or the first step of that cycle (Smart et al., 1994; Babitt et al., 1997), intracellular caveolin trafficking could be the key to understanding cellular cholesterol homeostasis.

Accumulating evidence suggests that caveolins may act as cholesterol sensors, and therefore as modulators of a wide range of cellular functions. Cav-1 expression is regulated at the transcriptional level by cholesterol (Bist et al., 1997). Niemann-Pick disease type C (NPC)[1] is an autosomal recessive lipid storage disorder, caused by mutations in the NPC1 protein and characterized by the accumulation of unesterified cholesterol in late endosomal compartments (for a review see Liscum, 2000). Cav-1 protein levels are increased several-fold in NPC1 heterozygotes, but homozygotes show only slightly increased cav-1 levels despite greatly increased unesterified cholesterol levels (Garver et al., 1997). This suggests that NPC1 may act indirectly as a regulatory factor of cav-1 expression. NPC1 is a multispanning membrane protein that contains a sterol-sensing domain that is homologous to the transmembrane domain of sterol-regulatory element-binding protein (SREBP)-cleavage activating protein (SCAP) (Brown and Goldstein, 1997). SCAP responds to low cholesterol levels by activating SREBP cleavage from the membranes of the ER (Hua et al., 1996). In human skin fibroblasts, SREBP-1 was described as a transcriptional inhibitor of caveolin gene expression (Bist et al.,

---

[1]*Abbreviations used in this paper:* BFA, brefeldin A; CDV, cav^{DGV} enriched vesicles; FC, free cholesterol; GFP, green fluorescent protein; NPC, Niemann-Pick disease C; PDI, phosphodisulphide isomerase; PM, plasma membrane; SCAP, SREBP-cleavage activating protein; SREBP, sterol-regulatory element-binding protein; YFP, yellow fluorescent protein.

1997). Intriguingly, there is also homology between NPC1 and the sterol sensing domain of Patched, the membrane receptor for Sonic hedgehog (Marigo et al., 1996), which itself contains a cholesterol moiety (Porter et al., 1996).

Caveolin and cholesterol have been linked to numerous signaling processes (see for a recent review Kurzchalia and Parton, 1999), but is it is still unclear how the cholesterol/caveolin cycle affects these processes. Cholesterol is synthesized in the ER of all nucleated cells and transported to the plasma membrane (PM), in part by a nonvesicular pathway (Kaplan and Simoni, 1985; Urbani and Simoni, 1990). Cells also take up cholesterol by receptor-mediated endocytosis of LDL, which is transported through the endocytic compartment to late endosomes. From late endosomes cholesterol is transferred to the PM or to the ER (Spillane et al., 1995; Underwood et al., 1998). Moreover, cholesterol can be converted to cholesteryl ester by the ER resident enzyme acyl-CoA/cholesterol acyltransferase (ACAT) to form the ester storage pool of the cell. Plasma membrane caveolae have been proposed as ports for the efflux of free cholesterol (FC), de novo synthesized or LDL-derived, to extracellular acceptors and possibly to the rest of the plasma membrane (Smart et al., 1996; Fielding and Fielding, 1997). In addition, in steroidogenic tissues and liver or in transfected CHO cells, the caveolae resident scavenger receptor SR-B1 mediates not only the efflux of FC to HDL but the selective uptake of HDL-cholesteryl esters (Babitt et al., 1997). How cholesterol distributes to other intracellular membranes remains unknown, although the existence of lipid rafts not only on the plasma membrane but in some intracellular membranes has been suggested. For instance, it was shown that a cholesterol-dependent sorting of GPI-anchored proteins occurs in recycling endosomes (Mayor et al., 1998) which contain some raft components (Gagescu et al., 2000).

The intracellular trafficking itinerary of caveolin is still controversial. Conformational changes of the caveolin protein complicate the interpretation of its localization in different cellular pools (Dupree et al., 1993; Luetterforst et al., 1999). Cav-1 is a fatty acid and cholesterol-binding protein (Murata et al., 1995; Trigatti et al., 1999). Moreover, cav-1 and 2 form homo- and heterooligomers in a process promoted by cholesterol (Murata et al., 1995). Caveolins have been considered as integral "hairpin"-like proteins with an intramembrane region of 33 amino acids, although they have been also described associated with lipoprotein particles in the secretory pathway of exocrine cells (Liu et al., 1999) or in cytosolic complexes, together with cholesterol and HSP56 (Uittenbogaard et al., 1998). Caveolin has been suggested to transport cholesterol from the ER to the plasma membrane (Smart et al., 1996) in a process, at least in part, mediated by a cytosolic pool of caveolin associated with chaperone complexes (Uittenbogaard and Smart, 2000). Cav-1 and -2 are present in vesicles carrying sphingolipids and GPI-anchored proteins from the trans Golgi network to the plasma membrane of epithelial cells (Scheiffele et al., 1998). In addition, oxidation of cholesterol by cholesterol oxidase induces caveolin redistribution from the plasma membrane to the ER/Golgi complex (Smart et al., 1994). The early exocytic pathway also has been recognized as an intermediate on the caveolin cycling pathway and a putative cis-Golgi targeting motif was identified in the COOH terminus of the protein (Luetterforst et al., 1999).

In the present study we have investigated the role of caveolins in regulating intracellular cholesterol homeostasis using a caveolin dominant mutant with two interesting properties; firstly, it can not reach the plasma membrane but accumulates in an intracellular compartment, and secondly, it inhibits the signal transduced by H-Ras by modifying cholesterol distribution. Our results show that this mutant protein behaves as in integral membrane protein and associates with the limiting membrane of lipid droplets. The mutant protein perturbs lipid transport resulting in changes in FC distribution.

Materials and Methods

Plasmids

YFP, GFP, and HA-tagged cav^{DGV} (residues 54–151) and the equivalents for cav-1, HA-tagged cav-1^{DGI} (residues 82–178) and cav-2, HA-tagged cav-2^{DKV} (residues 67–162), HA-tagged cav^{LLS} (residues 75–151) and full-length YFP and GFP-tagged cav-3 were generated as described previously (Luetterforst et al., 1999). Full-length cav-1 VSVG and full-length cav-2 myc have been previously described (Dupree et al., 1993; Scheiffele et al., 1998). CFP-tagged ER marker was purchased from CLONTECH. Myc-tagged sialotransferase was provided by Dr. Tommy Nilsson (EMBL, Heidelberg, Germany). Mouse NPC1 was provided by Dr. Jean Wilson (University of Arizona, Tucson, AZ).

Cell Culture, Antibodies, and Reagents

Baby hamster kidney cells (BHK) were maintained in DME with 10% vol/vol FCS supplemented with 2 mM L-glutamine. Cells were transfected using lipofectamine Plus (GIBCO BRL) according to the manufacturer's instructions. Quantitation of expression using cav-1 VSVG-transfected cells and a polyclonal anticaveolin antibody suggested that transfected protein was present at levels 3–4 times higher than endogenous levels (data not shown). In some experiments, before and/or after transfection cells were treated with 4.5 μg/ml of U18666A (from a stock solution in water stored at −20°C for less than 3 months). In some experiments, cells were preincubated for 16 h before transfection in a medium containing 50 μg/ml of oleic acid (Calbiochem) conjugated with fatty acid free BSA (Calbiochem) and incubated in the same medium for the time of the transfection as described previously (Brasaemle et al., 1997).

Primary antibodies used in this work are summarized in Table I. Gold-conjugated protein A was provided by Dr. J. Slot (University of Utrecht, Utrecht, The Netherlands). Fluorescein, Cy3, and gold-conjugated secondary antibodies were from Jackson ImmunoResearch. HRP-conjugated secondary antibodies were from Zymed Laboratories.

3β-(2-diethylaminoethoxy)-androstenone (U18666A) is from BIO-MOL Research Laboratories. 4',6-diamidino-2-phenylindole, dihydrochloride (DAPI), lysoTracker, and Nile red were from Molecular Probes. Cycloheximide, Triton X-100, filipin, brefeldin A (BFA), nocodazole and cytochalasin D were purchased from Sigma Chemical Co. 4[^{14}C]cholesterol (specific activity, 50.0 Ci/mmol) was from Amersham Pharmacia Biotech. Human serum was from a healthy volunteer.

Immunofluorescence, Electron Microscopy, and Video Microscopy

Immunofluorescence. Cells were prepared for immunofluorescence microscopy as described previously (Luetterforst et al., 1999). In extraction experiments, confluent cells were incubated by immersion in 300 μl of cold 10 mM Tris, pH 7.5, 150 mM NaCl, 5 mM EDTA, 1% Triton X-100, and a mixture of protease inhibitors for 3 min on ice, washed in cold PBS, and were then fixed for 10 min in cold 4% PFA and an additional 30 min at room temperature and finally processed for immunofluorescence or electron microscopy. In other experiments, cells were pretreated before fixation with 5 μg/μl of BFA for 4 h, 100 μM of chloroquine for 2 h, 1.6 μM nocodazole for 1 h, 10 μM cytochalasin D for 1 h or with 10 μg/ml cycloheximide for 24 h.

Table I. Antibodies Used in This Work

Antibody	Specificity	Reference
HA	Mo	Prof. David James (University of Queensland, Queensland, Australia)
HA	Rb	Dr. Tommy Nilsson (EMBL, Heidelberg, Germany)
VSVG	Rb	Dr. Tommy Nilsson (EMBL, Heidelberg, Germany)
myc	Rb	Dr. Tommy Nilsson (EMBL, Heidelberg, Germany)
GFP	Rb	Prof. David James (University of Queensland, Queensland, Australia)
Caveolin 1	Rb	Transduction Laboratories (C13630)
Caveolin 1	Mo	Transduction Laboratories (C37120)
p23	Rb	Prof. Jean Gruenberg (University of Geneva, Geneva, Switzerland) (Rojo et al., 1997)
KDEL-receptor	Rb	Dr. Hans-Peter Hauri (Biozentrum, Basel, Switzerland) (Griffiths et al., 1994)
KX5	Rb	Dr. Steven Fuller (EMBL, Heidelberg, Germany)
PDI (KDDD)	Rb	Dr. Steven Fuller (EMBL, Heidelberg, Germany)
SKL	Rb	Zymed Laboratories (71-8400)
NPC1	Rb	Dr. Jean Wilson (University of Arizona, Tucson, AZ)
Sec61	Rb	Dr. Jean-Pierre Gorvel (CIMR, Marseille, France)
LBPA (6C4)	Mo	Prof. Jean Gruenberg (University of Geneva, Geneva, Switzerland) (Kobayashi et al., 1998)
Tubulin	Mo	Sigma Chemical Co. (T9026)

GM1 Internalization Assay. Transfected cells were rinsed in Air medium (10% FCS, Hanks minimal essential media (GIBCO), 0.75 mg/ml sodium bicarbonate, 10 mM Hepes, pH 7.4) and incubated in the same medium containing 10 mg/ml of sialoganglioside-GM1 (Sigma Chemical Co) at 37°C for 2 h. After fixing the cells with 4% PFA, coverslips were incubated for 30 min in a blocking solution (0.2% BSA, 0.2% fish skin gelatin diluted in PBS) containing 1 μg/ml of cholera toxin FITC conjugated (Sigma Chemical Co).

Nile Red Staining. Cells were transfected by electroporation (300 V, 125 μF at 25°C) and plated on coverslips and labeled with mAbs to HA, followed by Cy3-conjugated secondary antibodies, and finally mounted in mowiol containing Nile red (1:1,000 from a saturated stock solution in acetone). Transfected cells were selected for the presence of rings in the red channel and the corresponding image in the green channel was captured. Then, the samples were exposed for 30 s in the red channel (to quench the presence of lipid dye in the red channel) before the corresponding image was captured. To quantitate the relative amounts of Nile red labeling in transfected and nontransfected cells, fields were selected that contained an example of each. Using NIH image software, the mean pixel intensity per unit area of one of each cell type was assayed. The nontransfected control cell was then given a base value of 1.00 and the relative pixel intensity of the transfected cell was expressed as a factor. This was repeated in 14 different random fields allowing an average difference to be calculated.

Filipin Staining. Filipin staining was performed as outlined previously (Carozi et al., 2000).

Preembedding Labeling of Triton X-100 Extracted Cells. GFP-tagged cav^{DGV}-transfected cells were extracted with Triton X-100 as described, and were then fixed with 4% PFA, 0.02% glutaraldehyde in KoAc for 10 min, quenched, and blocked as above. Cells were labeled with antibodies for GFP diluted in blocking solution for 1 h, extensively washed with PBS and were then incubated with gold-conjugated protein A for 2 h. Then the cells were washed for 30 min in PBS and fixed with 1% glutaraldehyde in 100 mM cacodylate buffer for 1 h and processed for Epon embedding in the dish by standard procedures as described previously (Parton, 1994). Sections were cut parallel to the culture dish.

Lowicryl and Frozen Sectioning. BHK cells were embedded in Lowicryl HM23 resin after fixation in 1% glutaraldehyde in 100 mM cacodylate buffer. They were then processed exactly as described previously (Parton, 1994) with the modification that the cells were embedded in Lowicryl HM23 rather than HM20. Frozen sections were prepared as described previously (Luetterforst et al., 1999). Frozen and Lowicryl sections were labeled according to standard techniques (Parton, 1994).

Time-lapse Video Microscopy. BHK cells were transfected with GFP-tagged cav^{DGV}. After 18 h the growth media was replaced with Air medium. The cells were observed in an Olympus BX60 microscope with a 60× water immersion lens, and the images were captured using IP Lab software with a CCD camera (Hamamatsu). Images were captured automatically at intervals ranging from 10 s to 1 min. Dual color movies were made with the addition of lysoTracker to a final concentration of 50 nM in Air media in 35-mm dishes of BHK cells transfected with GFP-tagged cav^{DGV} for 24 h. Then, the automatic capture was set at 20 s intervals. After the automatic capture in the first channel, another image was immediately captured in the second channel with a delay of 2 s. IP Lab software was then used to produce composite images, which could then be animated. All images were further processed using Adobe Photoshop 5.0 to enhance contrast and adjust the apparent intensity in the dual color movie.

Cell Fractionation and Western Blotting

Confluent 10-cm dishes of transfected BHK were washed twice with cold PBS before being scraped into ice-cold 10 mM Tris, pH 7.5, 150 mM NaCl, 5 mM EDTA, and a mixture of protease inhibitors. Cells were homogenized by passing through a 22-gauge needle 25 times at 4°C. In some experiments, cells were scraped in 0.5 M Na$_2$Co$_3$, pH 11.5, and in this case homogenized by passing them through a 22-gauge needle 10 times at 4°C. In other experiments the homogenization buffer contained 1% Triton X-100 and the cells were homogenized by passing through a 22-gauge needle 10 times at 4°C. Nuclei and unbroken cells were removed by centrifugation at 5,000 rpm in a TLS-55 rotor (Beckman) for 5 min at 4°C. The resulting supernatant was centrifuged at 75,000 rpm in a TLA-100 rotor (Beckman) to separate membranes (p75) from soluble proteins (sol). Finally, the pellets were resuspended in homogenization buffer and sonicated to make them soluble. Fractions were stored at −20°C before processing. Western blotting was performed as described previously (Pol et al., 1999). Protein was quantified by BCA Protein Reagent Assay kit (Pierce Chemical Co.).

Cholesterol Efflux and Biosynthesis Analysis

Cos-1 cells were grown in DME supplemented with 10% FBS and 100 U/ml penicillin and 100 μg/ml streptomycin. Cells were seeded in 24-well plates or 35-mm plates for 20 h before transfection in COS-1 medium. The cells at ~70% confluency were transfected with 1 μg of cav^{DGV} HA in pCB6 or vector alone with Fugene-6 according to the manufacturer's instructions. 3 h after transfection the medium was replaced by COS-medium containing [^{14}C]cholesterol (100 nCi/ml) and incubated for further 45 h. Then cells were processed by analysis of cholesterol biosynthesis as previously described (Heino et al., 2000) or cholesterol efflux. To quantify cholesterol efflux cells were then incubated for 3 h in the absence of label, washed twice with PBS, and once with serum-free DME, and efflux was carried out in 500 μl of DME containing 20% human serum for 2 h. The medium was collected and cells were recovered by dissolving in 0.2 M NaOH. Aliquots of the cells and medium were analyzed by liquid-scintillation counting to determine the [^{14}C]cholesterol content.

Online Supplemental Material

Online supplemental materials can be found at http://www.jcb.org/cgi/content/full/152/5/1057/DC1. Time-lapse video microscopy: Video 1 corresponds to Fig. 4 a. Cav^{DGV} vesicles are immobile and nonacidic vesicles (real time 28 min). Video 2 corresponds to Fig. 4 b. Cav^{DGV} transits the tubules of the ER and accumulates in a stable compartment (real time 100 min). Video 3, corresponds to Fig. 4 c. High magnification of the CDV compartment formation (real time 125 min).
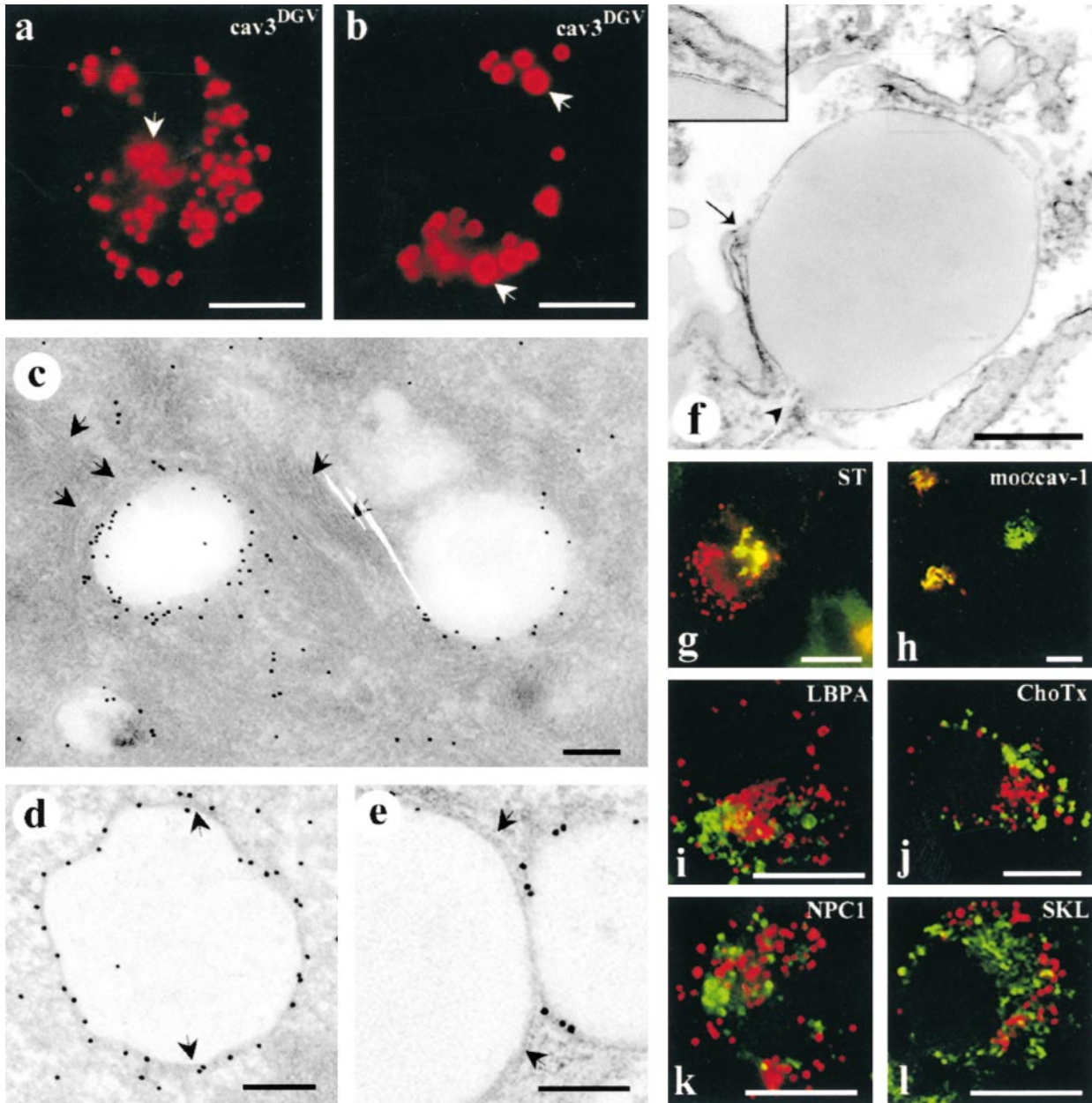
Figure 1. Cav^{DGV} is targeted to the membrane of intracellular vesicular structures. a, BHK cells were transfected with HA-tagged cav-3^{DGV} for 24 h and were then labeled with antibodies to HA tag, followed by specific Cy3-conjugated secondary antibodies. Cav^{DGV} mainly located in enlarged intracellular rings, and some protein was detected in the tubular elements of the ER (see Fig. 2) and in the perinuclear region (arrows and g and h). b, BHK cells were transfected with HA-tagged cav^{DGV} for 24 h and were then treated with 5 μg/ml of cycloheximide for an additional 24 h. After blocking of protein synthesis, the truncated protein was exclusively detected in very enlarged intracellular vesicles (arrows). c, BHK cells were transfected with GFP-tagged cav^{DGV} and frozen sections were processed for immunoelectron microscopy using anti-GFP antibodies, followed by protein A–gold. The mutant protein was detected enriched on the membrane of electron-lucent vesicles of 300–500-nm diam, often surrounded by intermediate filaments (arrows). d and e, Lowicryl sections (of freeze-substituted/low temperature embedded sections) of GFP-tagged cav^{DGV}-transfected cells labeled with antibodies to GFP followed by protein A–gold. Cav^{DGV}-containing vesicles (CDV) comprise a membrane bilayer (see arrows in d and e) surrounding a putative lipid-filled area. f, Epon sections showing a morphologically similar structure connected to tubular elements possibly corresponding to the ER (arrow and arrowhead), which were frequently observed in nontransfected cells. The typical morphology of lipid-filled body enclosed by a bilayer structure (see insert) is readily observed in epon sections. g, BHK cells were cotransfected with myc-tagged sialotransferase (a specific marker for trans Golgi) and HA-tagged cav^{DGV} and the distribution of the proteins studied by immunofluorescence by means of antitag specific antibodies. The distribution of sialotransferase (green) and cav^{DGV} (red) clearly overlapped in the Golgi area, however CDV rings did not contain the Golgi marker. h, HA-tagged cav^{DGV}-transfected cells were label with an mAb to cav-1 (which exclusively recognizes the Golgi complex conformation of cav-1) and a polyclonal antibody to HA-tag. When cav^{DGV} (red) accumulated in the Golgi region, the truncated protein clearly colocalized with the Golgi complex-associated pool of endogenous cav-1 (green). i and l, HA-tagged cav^{DGV}-transfected cells were labeled with polyclonal antibodies to the peroxisome marker SKL (l) or the late endosome marker, lysobisphosphatidic acid (h) and with an mAb to the HA-tag. The endosome and peroxisome markers (green) were excluded from the CDV compartment (red). j, Cav^{DGV}-transfected cells were incubated for 2 h at 37°C with 10 μg/ml of GM1 to allow insertion of the ganglioside into the plasma membrane and internalization. GM1, detected by using 1 μg/ml of Cholera toxin–FITC, was completely excluded from the CDV compartment (red). k, BHK cells were cotransfected with Niemann-Pick C1 protein and cav^{DGV} for 24 h and were then labeled with a polyclonal antibody to NPC1 and the mAb to the HA tag. Transfected NPC1 (green) does not colocalize with the CDV vesicles (red). Bars: (a, b, and g–l) 5 μm; (c–f) 100 nm.

Results

Cav^DGV Is Targeted to the Limiting Membrane of Intracellular Spherical Structures, but Not to the Plasma Membrane

To examine the intracellular itinerary of caveolin and its role in cholesterol homeostasis, we studied the intracellular location of the cav^{DGV} mutant, a truncated protein that acts as a dominant negative inhibitory mutant through an effect on cholesterol. Cav^{DGV} is a deletion of cav-3, which lacks the first 53 residues of the protein but contains an intact scaffolding domain. This mutant protein localizes to an apparently novel nonendocytic intracellular compartment. COOH-terminally HA-tagged cav^{DGV} was expressed in BHK cells and its distribution analyzed by immunofluorescence microscopy. The protein showed a characteristic staining of large intracellular rings (Fig. 1, a and b). Identical results were obtained when NH$_2$-terminally GFP or COOH-terminally YFP-tagged cav^{DGV} was expressed (see below). Often rings of different sizes and complexes of two or more vesicles could be observed (Fig. 1 a). In addition, some labeling was observed in tubular elements, characteristic of the ER (see later) and in the Golgi region (Fig. 1 a, arrow; also see Luetterforst et al., 1999), but after cycloheximide treatment only the ring-like staining was observed in very enlarged vesicles (Fig. 1 b, arrows). This strongly suggests that the steady state distribution of this mutant protein is the ring-like structures. Consistent with previous results (Roy et al., 1999), cav^{DGV} was not detected on the plasma membrane, even using the YFP or GFP-tagged construct, suggesting that the lack of surface labeling is not due to inaccessibility of epitopes.

To further characterize the properties and origin of the cav^{DGV} compartment, we performed electron microscopy on cav^{DGV}–GFP-expressing cells. Frozen sections provided high labeling efficiency (Fig. 1 c) and showed labeling for the mutant protein surrounding an electron lucent area,

reminiscent of a lipid droplet. Cav^{DGV} containing vesicles were often surrounded by intermediate filaments (see arrows in Figs. 1 c and 5 d). However, the frozen sections did not provide good membrane preservation in the area of the cav^{DGV}-labeled structures. We therefore employed a freeze-substitution/low temperature embedding approach that has been optimized for retention and high resolution localization of lipids (van Genderen et al., 1991; Voorhout et al., 1991; Parton, 1994). The HM23 lowicryl sections of cav^{DGV}-transfected cells were labeled with antibodies to GFP, followed by protein A-gold. Labeling was observed on large spherical electron-lucent structures of 300–500-nm diam (Fig. 1, d and e) which were enclosed by a clearly defined membrane (arrows). The morphology of the labeled elements suggested that the cav^{DGV} mutant is specifically targeted to the limiting membrane of a membrane-enclosed compartment containing lipids. Structures with identical morphology were observed in nontransfected cells (Fig. 1 f). Those structures were often closely associated with tubular elements (Fig. 1 f, arrow and arrowhead) presumably corresponding to the ER.

Cav^DGV Accumulates in a Subcompartment of the ER

Our previous studies (Roy et al., 1999) suggested that the cav^{DGV} vesicles (here operationally abbreviated to CDVs for Cav-DGV–labeled vesicles) lack endosomal markers, but the molecular nature and origin of these vesicles was unknown. Therefore, we carried out a series of labeling experiments to examine the nature of this compartment. The Golgi complex, late endosomes, and the ER have all been described as intermediate steps in the intracellular trafficking of cholesterol and caveolin has been described previously in the Golgi network (Kurzchalia et al., 1992). Epitope-tagged sialotransferase, a specific marker of the trans-Golgi, was cotransfected with cav^{DGV} in BHK cells. Although the markers overlapped in the Golgi region, the proteins did not colocalize in the characteristic CDVs (Fig.
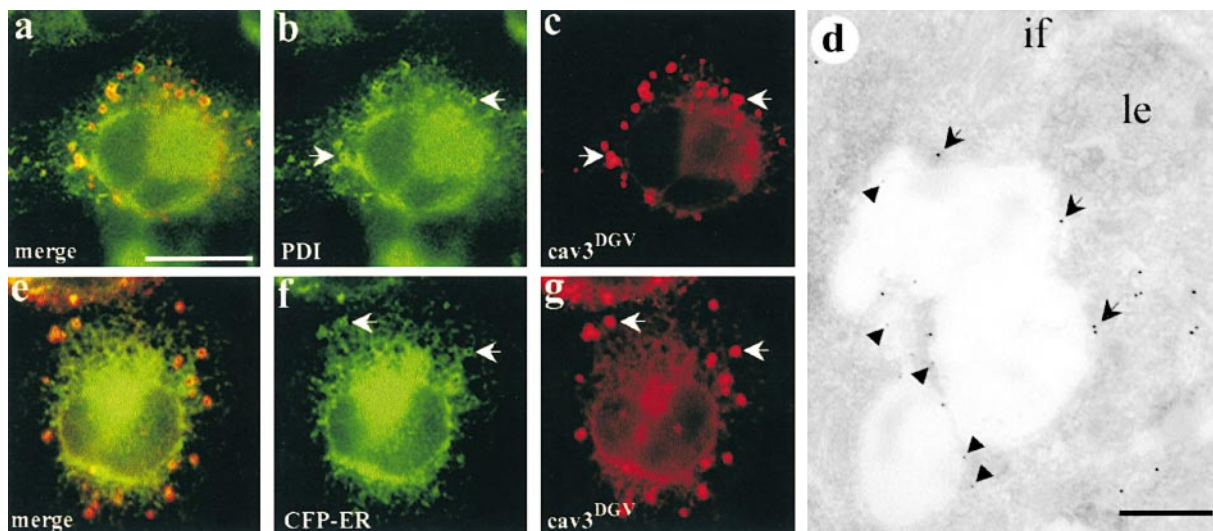

Figure 2. CDV rings contain markers for the ER. a–d, BHK cells were transfected with cav^{DGV} for 24 h, and were then labeled with a polyclonal antibody to PDI (a marker for the ER) and an mAb to the HA tag. PDI (green) was located in the reticular network characteristic of the ER (b) and in some vesicular structures that colocalized to some extent with CDV rings (red) (b and c, arrows). The colocalization between both proteins was corroborated in frozen sections of cav^{DGV}-transfected cells (d) labeled with the same antibodies, followed by anti-rabbit antibodies conjugated to 15-nm gold (arrows) and anti-mouse antibodies conjugated to 5-nm gold (arrowheads). e–g, BHK cells were double transfected with CFP-tagged ER marker and HA-tagged cav^{DGV}. The cells were labeled with a polyclonal antibody to GFP (to increase the signal) and the mAb to HA tag (e). Clear colocalization could be observed between some of the CDV rings (red) and the ER marker (green) (f and g, arrows). Bars: (d) 100 nm; (a–e) 5 μm.
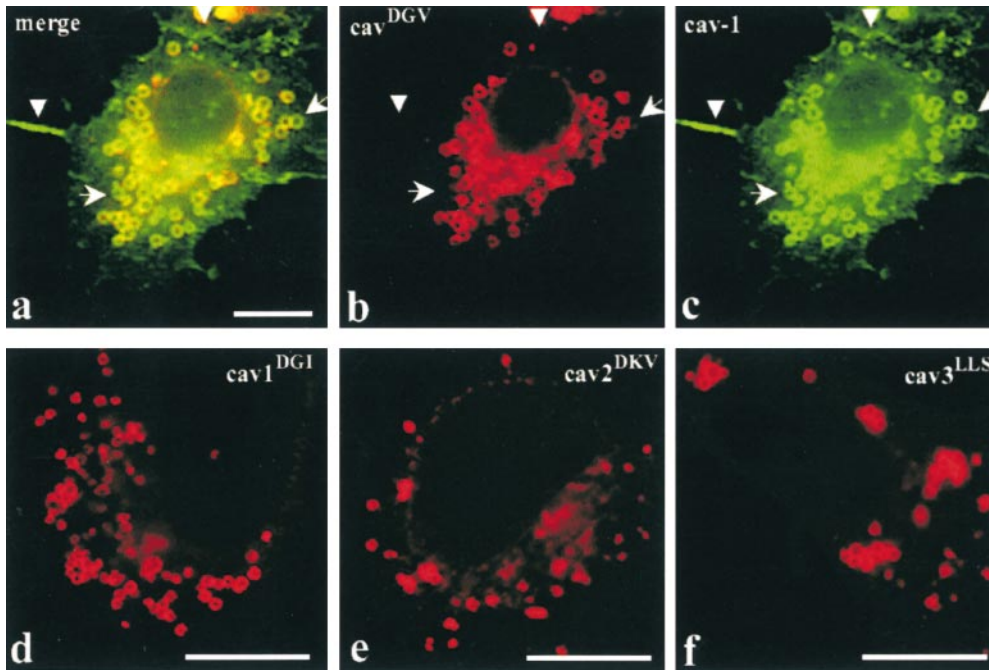
Figure 3. The cav^{DGV} phenotype is a feature of all caveolin family members. a–c, BHK cells were cotransfected with full-length VSV-G–tagged cav-1 and HA-tagged cav^{DGV}, and after 24 h were labeled with a rabbit antibody to VSV-G tag and a mouse antibody to HA tag. In a low but significant proportion of transfected cells (2–5% of transfectants) full-length cav-1 (green) accumulated in the same intracellular rings as cav^{DGV} (red). Although in those cells, cav-1 was detected on the PM (a and c, arrowheads) cav^{DGV} was totally excluded from the PM. Some ring-like structures were strongly labeled for full-length cav-1 but not for cav^{DGV} (b and c arrows). d and e, BHK cells were transfected with HA-tagged cav-3^{DGV} equivalent truncation mutants of cav-1 (cav-1^{DGI}, d) and cav-2 (cav-2^{DKV}, e) and the cells labeled with mouse anti-HA tag. Both equivalent mutants accumulated in morphologically identical rings to cav-3^{DGV}, demonstrating that the CDV compartment is a general characteristic of all the caveolin family members. f, BHK cells were transfected with HA-tagged cav-3^{LLS} (a cav-3 truncation lacking the entire NH$_2$-terminal domain up to the putative intramembrane region) and labeled with mouse anti-HA tag. Cav-3^{LLS} accumulated, as cav-3^{DGV}, in CDV-like structures, showing that the caveolin scaffolding domain is not involved in the targeting of the protein to this compartment. Bars, 5 μm.

1 g). The same colocalization was observed when cav^{DGV}-transfected cells were label with an mAb to cav-1 (which exclusively recognizes the Golgi complex conformation of cav-1, but not cav^{DGV}). When cav^{DGV} accumulated in the Golgi region, the truncated protein clearly colocalized with the Golgi complex-associated pool of endogenous cav-1 (Fig. 1 h). In view of the lipidic nature of the internal core of the CDVs, as visualized by electron microscopy, we examined the distribution of lysobisphosphatidic acid (LBPA), a lipid that is highly enriched in late endosomes (Kobayashi et al., 1998), and the ganglioside GM1, which was incorporated into the plasma membrane and internalized for 2 h at 37°C to label the endocytic system. Neither marker colocalized with the caveolin mutant (Fig. 1, i and j). NPC1, which plays a vital role in cholesterol transport, has been suggested to associate with both endosomal and nonendosomal compartments (Garver et al., 2000). However, NPC1 was also excluded from the CDVs (Fig. 1 k).

We then carried out a series of colocalization studies of cav^{DGV} with markers of other compartments, including a peroxisomal marker (SKL, Fig. 1 l) and four ER specific markers (Sec61, Kx5, KDEL-R, and PDI). Of these markers, only two, PDI (Fig. 2 a, and arrows in b and c) and KDEL-R (not shown), colocalized to some extent with DGV vesicles, suggesting that the vesicles were derived from the ER. Colocalization between DGV and PDI was confirmed by electron microscopy studies in frozen sections of cav^{DGV}-transfected cells (Fig. 2 d). To examine this further, BHK cells were cotransfected with cav^{DGV} and a fluorescently tagged ER marker. Clear colocalization was observed between some of the ring-like CDVs and the ER marker (Fig. 2 e, and arrows in f and g). We conclude that although cav^{DGV} can transit the Golgi network and the tubular elements of the ER, the steady state distribution of the protein is a subcompartment of the ER.

The cav^{DGV} Compartment Is Accessed by all the Known Caveolin Family Members

We next investigated whether the CDVs might be a general feature of the caveolin cycling pathway by examining whether full-length caveolins can access this compartment. Cav^{DGV} was coexpressed with full-length cav-1, 2, or 3. Full-length caveolins distributed in a similar manner to endogenous cav-1 and the protein could be detected on the PM, in the Golgi region of the cells, and showed limited colocalization with the cav^{DGV} mutant protein (not shown). Extensive colocalization was observed in only a low but significant percentage of the cav^{DGV} mutant expressing cells (2–5%, see Fig. 3 a). Full-length caveolins can reach both the PM and the CDVs but cav^{DGV} is totally excluded from the PM (see arrowheads in Fig. 3, b and c). Notice that not all the cav-1 positive rings contained cav^{DGV} (compare Fig. 3, b and c, arrows), suggesting that the formation of CDV is not exclusively induced by the presence of the mutant protein (see also Fig. 1 f). Since cav-1 does not oligomerize with cav-3, these results suggest that CDVs may be accessed by wild-type caveolins under physiological conditions.

We then constructed the equivalent truncation mutants of cav-1 (cav-1^{DGI}) and cav-2 (cav-2^{DKV}). Fig. 3, d and e, show that cav-1^{DGI} and cav-2^{DKV} accumulated in morphologically identical compartments to cav-3^{DGV}. We then investigated whether the caveolin scaffolding domain was
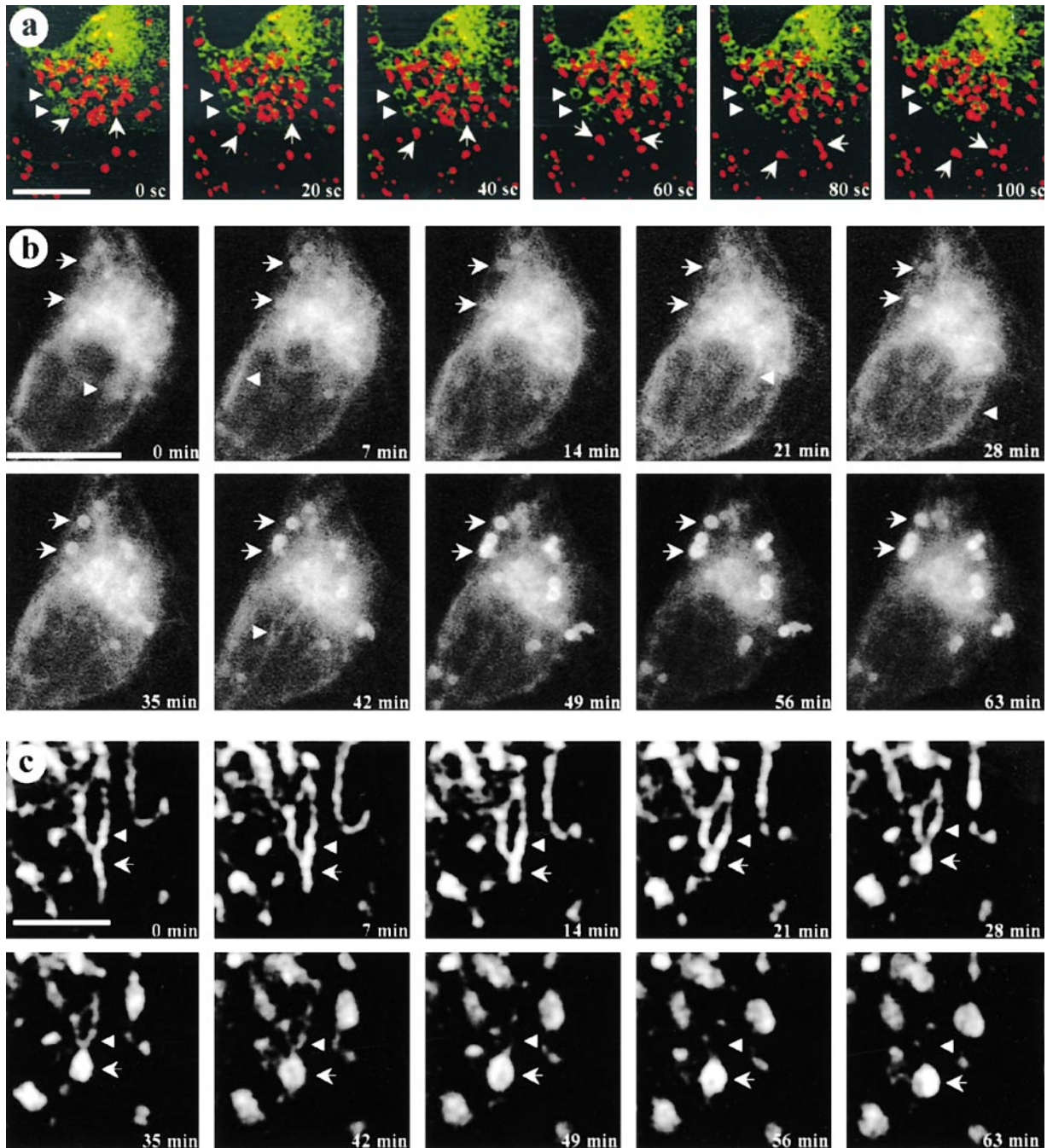
Figure 4. Real-time microscopy. CDV are immobile structures formed by maturation processes in some specific regions of the ER. a, Living GFP-tagged cav[DGV]-transfected cells were incubated in a medium containing a marker for acidic compartments, lysoTracker. Cells expressing GFP-cav[DGV] were selected under the microscope and the focus was kept constant. Images of both channels (green/red) with a delay of 10 s between channels were captured over 5 min. The figure shows a selected sequence of 6 consecutive frames (20-s interval between images) representing a total period of 100 s. LysoTracker-labeled vesicles showed a rapid bidirectional motility (arrows) but cav[DGV]–GFP positive vesicles showed no significant motility in any axis (arrowheads). b and c, In an attempt to capture the formation of CDVs, cells were transfected with GFP-tagged cav[DGV] for 18 h and were then observed by video microscopy. Cells were selected for the presence of forming rings (see arrows in the first panel) and the focus was kept constant during the entire experiment. Images were captured with a constant interval of 7 min. The figure shows a selected sequence of 10 consecutive frames representing a total period of 63 min. At time 0, cav[DGV]–GFP was abundant in the tubular elements of the ER and in the Golgi area. Progressively the protein is less abundant in the ER and Golgi complex and accumulates in the forming rings (arrows) to shape well-defined CDV ring-like structures in ∼60 min. c shows a selected high magnification example of CDV formation. The protein can be detected moving in waves along the tubules of the ER (arrowheads) until the formation of the DGV-containing vacuolar structures (arrows). Bars: (a and b) 5 μm; (c) 1 μm. Supplemental videos are available at http://www.jcb.org/cgi/content/full/152/5/1057/DC1.

required for accumulation in this compartment. From Fig. 3 f, it is apparent that removal of the entire NH_2 terminus of cav-3 up to the putative intramembrane region (cav-3^{LLS}) resulted in labeling of morphologically identical structures. We conclude that the cav^{DGV}-containing vesicles are accessed by all the caveolin family members and that the caveolin scaffolding domain is not involved in the targeting of the protein to this compartment.

Cav^{DGV} Vesicles Are Immobile, Nonacidic Vesicles whose Formation Is Sensitive to Brefeldin A

We then tested whether the CDVs were acidic. Lyso-Tracker, a marker for acidic compartments, did not label the CDVs. The different properties of the two sets of vesicles was further established by dual color real-time video microscopy (Fig. 4 a). The lysoTracker-labeled vesicles showed rapid bidirectional motility (up to 5 μm/min; Fig. 4 a, arrows) consistent with microtubule-based motility of late endosomes and lysosomes, as described previously. In contrast, the cav^{DGV}-GFP-labeled vesicles showed no significant motility in any axis, remaining focused during the whole experiment (Fig. 4, arrowheads). Interestingly, the lysoTracker-positive vesicles showed less motility in regions of the cell close to rings in comparison with those in the periphery of the cells or in nontransfected cells.

We then used this system to investigate the origin of the CDVs. Cells were transfected with GFP-tagged cav^{DGV} for 18 h and observed by video microscopy. Fig. 4 b shows a sequence of ten pictures captured every seven minutes from a cav^{DGV} expressing cell. As in previous experiments, the focus of the microscope was kept constant during all the experiment and all the frames were equally analyzed. The cells to study were selected for the presence of forming rings (see arrows in the first panel of Fig. 4 b). In cells selected by these criteria, cav^{DGV} appeared concentrated in the perinuclear area (around the nucleus and in characteristic tubular elements), presumably corresponding to the ER. Subsequently, cav^{DGV} progressively accumulated in the forming structures to finally define a well-shaped ring in ~60–90 min. In accordance with the above results (Fig. 4 a), the swelling of the compartment occurs without any appreciable change in the original position of the ring (see arrows). During the entire sequence, cav^{DGV} could be observed moving in "waves" along the tubules of the ER (see arrowheads). In some cases, it was observed that these tubules fused with preexisting CDVs (see arrowheads in Fig. 4 c). After an average of 90 min, the ER-associated staining of CDVs became less apparent and few changes could be observed after that time in relation to the formation of the rings. Together, these results suggest that cav^{DGV} transits the tubules of the ER and accumulates in a nonacidic and stable compartment that originates and matures in some specific regions of the ER.

Ultrastructural and Biochemical Characterization of cav^{DGV} and the cav^{DGV} Vesicles

We further investigated the properties of the CDVs. Transfected BHK cells were incubated in a medium containing 5 μg/ml of BFA for 4 h. BFA treatment induced a dramatic tubulation of Golgi stacks labeled with p23, however CDV rings were completely resistant to the treatment once

formed (Fig. 5 a). Then, transfected BHK cells were extracted, before fixation, at 4°C in a buffer containing 1% Triton X-100. Cav^{DGV} distribution was then examined by immunofluorescence and electron microscopy. Cav^{DGV} in CDVs, but not cav^{DGV} in Golgi or in tubular elements of the ER, was resistant to preextraction with detergent as judged by immunofluorescence (Fig. 5 b). When the cells were pretreated before extraction with nocodazole (Fig. 5 c) or cytochalasin D (not shown) and were then analyzed by immunofluorescence, CDVs remained unextracted indicating that resistance to extraction with detergents is not due to the association of CDVs with elements of the cellular cytoskeleton. The same labeling scheme was used for electron microscopy using anti-GFP antibodies, followed by protein A-gold to detect the tagged mutant protein. The extraction procedure removed most of the visible internal membranes including the nuclear envelope (Fig. 5 e, arrows) and mitochondrial membranes, but the plasma membrane was largely intact. Labeling for the caveolin mutant was observed on large ring-shaped structures corresponding to the CDVs (Fig. 5, d and e) often surrounded by intermediate filaments (Fig. 5 d, arrows). At higher magnification the gold particles were shown to associate with striking electron dense filamentous aggregates on the cytoplasmic face of the CDVs (Fig 5, d and e, arrowheads). The nature of these aggregates remains unknown at the present time. In addition, no protein was detected on the membrane of vesicles corresponding to the rough ER (Fig. 5 d, asterisk).

In view of the retention of the CDVs after detergent treatment and its putative ER origin, we examined whether other markers of the ER are resistant to Triton extraction. After extraction of nontransfected cells, PDI labeling was extensively reduced from the characteristic ER network to sparse vesicular elements (not shown), demonstrating the existence of detergent-resistant domains of the ER in normal cells. When the same experiment was performed in cav^{DGV}-transfected cells, those vesicles were strongly labeled with both cav^{DGV} and PDI (Fig. 5 f). Moreover, the size of the detergent resistant PDI domain was increased, suggesting that the expression of cav^{DGV} induced the enlargement of the ER subdomain.

The cav^{DGV} protein retains the putative intramembrane domain of the wild-type protein, but caveolin has also been suggested to exist in a soluble form (Uittenbogaard et al., 1998). To examine whether cav^{DGV} is membrane-associated, transfected cells were treated with pH 11 sodium carbonate. The mutant protein, like the wild-type protein in these cells, was resistant to carbonate treatment (Fig. 5 i). However, in contrast to full-length caveolin, the cav^{DGV} mutant was soluble after extraction with detergent in this biochemical assay. This contrasts with the lack of extraction of the mutant protein in intact cells as judged by immunofluorescence microscopy and suggests that the protein is in a nonraft environment, but in the intact cell this domain is retained through nonlipidic interactions.

Cav^{DGV} Associates with a Neutral Lipid-containing Organelle and Induces Lipid Accumulation

Cav^{DGV} specifically inhibits H-ras function through an effect on cholesterol at the plasma membrane. Therefore, we examined whether cav^{DGV} had functional effects on lipid
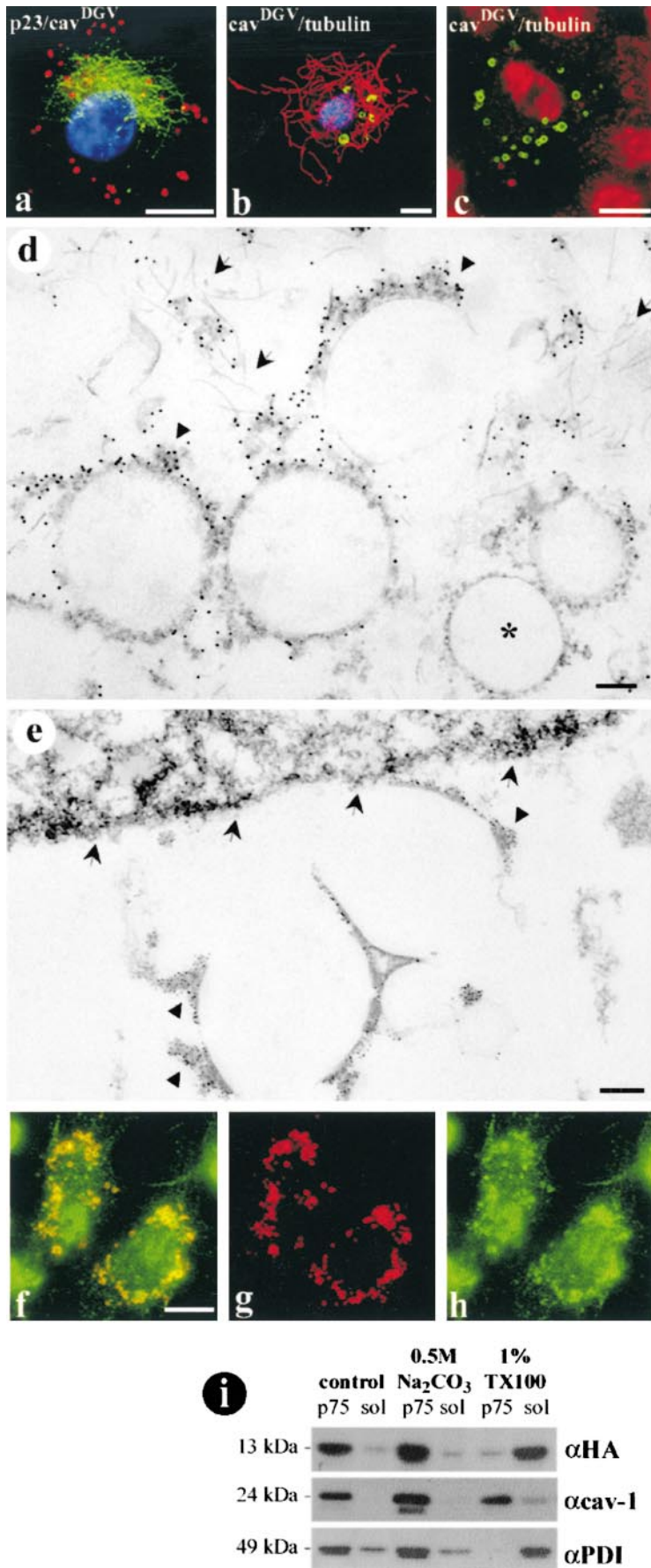
Figure 5. Biochemical and morphological characterization of the CDV compartment. a, HA-tagged cav[DGV] expressing cells were incubated in a medium containing 5 µg/ml of BFA for 4 h and were then labeled with a polyclonal antibody to p23 (a cis Golgi marker) and an mAb to the HA tag, followed by secondary antibodies and finally incubated with DAPI to visualize the resistant cells. BFA treatment induced a dramatic tubulation of Golgi stacks (green), however CDV rings (red) were completely resistant to the treatment. b and c, HA-tagged cav[DGV]-transfected cells were incubated before fixation in a tris-buffered medium containing 1% Triton X-100 at 4°C for 3 min and were then fixed and labeled with an mAb to β-tubulin and a polyclonal antibody to HA tag, followed for secondary antibodies and DAPI to visualize the resistant cells. The CDV compartment (green) and the microtubule network (red) were both resistant to the extraction with the detergent. When the cells were pretreated in a medium containing 1.6 µM nocodazole for 4 h and were then extracted with the detergent, the microtubule network appeared completely disorganized in a very diffuse cytoplasmic staining (compare c with b) but CDV rings remained resistant to the detergent. d and e, Epon sections of detergent extracted GFP-tagged cav[DGV]-transfected cells were labeled with antibodies to GFP followed by protein A–gold before embedding. Cav[DGV] was detected in electron-dense aggregates (arrowheads) on the membrane of CDV ring-shaped structures surrounded by a network of intermediate filaments (arrows in d). Other internal membranes like the nuclear envelope (arrows in e) or mitochondrial membranes were solubilized. The membranes of the rough ER did not contain cav[DGV] (asterisk in d). f–h, Cav[DGV]-transfected cells were extracted with 1% Triton X-100 at 4°C for 3 min and were then labeled with an mAb to HA tag and a polyclonal antibody to PDI. Some domains of the ER were resistant to the extraction with detergents (h, compare with Fig. 2 e) and clearly colocalized with cav[DGV]. i, Cav[DGV]-transfected cells were homogenized at 4°C in a Tris buffered solution or in Tris buffered solution containing pH 11 0.5 M NaCO₃ or 1% Triton X-100. Then, a postnuclear supernatant of each treatment was centrifuged at 75,000 rpm for 30 min to separate membrane associated proteins (p75) or soluble proteins (sol). 5 µg of protein of each sample were resolved by SDS PAGE electrophoresis, transferred to p-immobilon membranes and the presence of HA, cav-1, and PDI detected by Western blotting by means of specific antibodies. The three studied proteins were associated with the membrane fraction of the cells homogenized in the control buffer and in the buffer containing NaCO₃. Although cav-1 was resistant to the solubilization with 1% Triton, HA and PDI were solubilized. Bars: (d and e) 100 nm; (a–c and f) 5 µm.
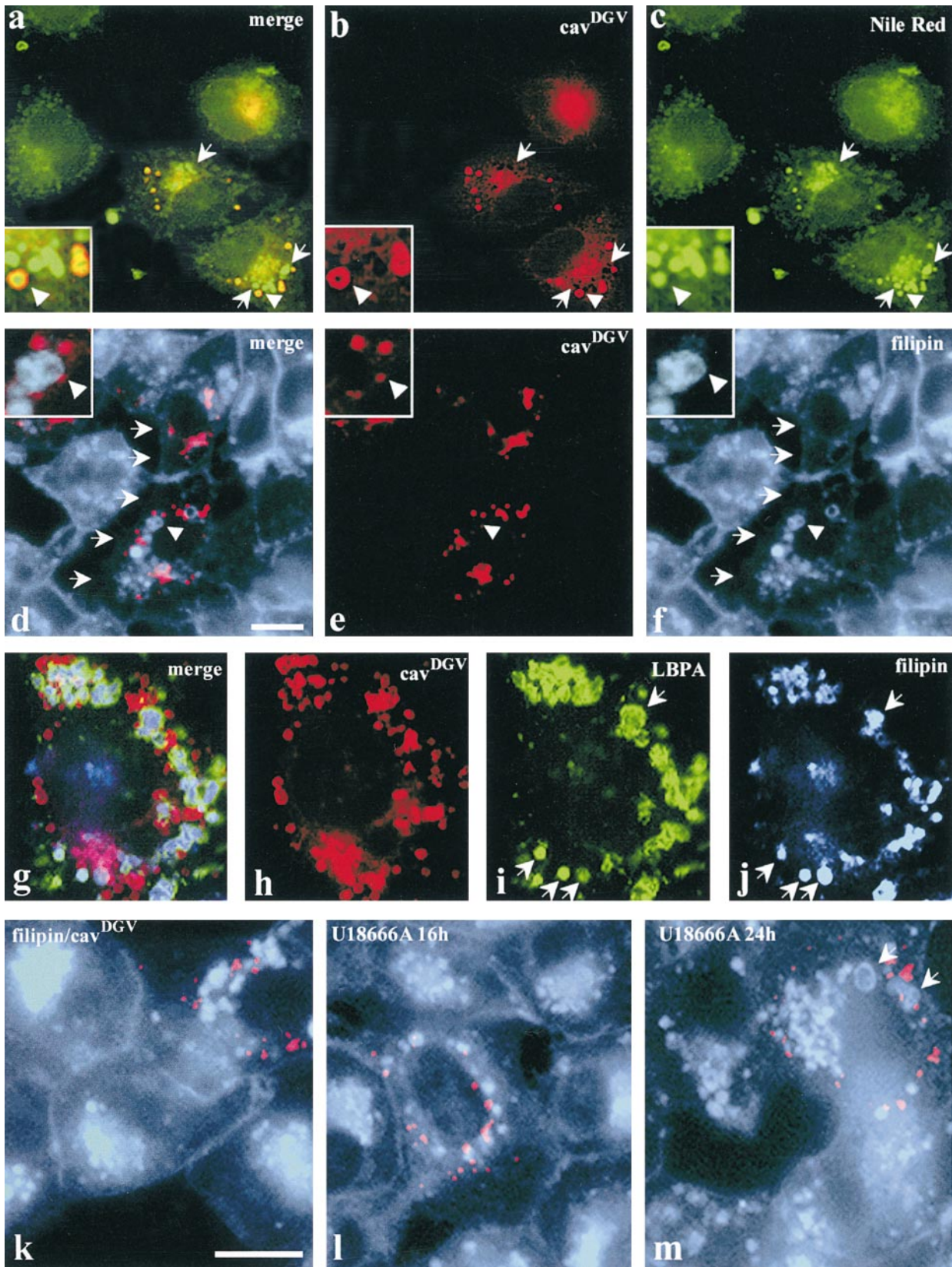
Figure 6. CDV is a lipid-enriched compartment and cav^{DGV} expression induces lipid accumulation. a–c, Cav^{DGV} HA-tagged transfected cells were labeled with mAbs to HA, followed by Cy3-conjugated secondary antibodies. The samples were mounted in mowiol, containing a solution of the lipid probe, Nile red. The cells were selected for the presence of rings in the red channel and the corresponding image in the green channel was captured. Then the samples were exposed for 30 s in the red channel before the corresponding image was captured. Nile red staining was within the center of CDVs, whereas cav^{DGV} formed the characteristic ring around the vesicle (arrow-

distribution. Cav^{DGV}-transfected cells were labeled with the neutral lipid probe, Nile red. When cav^{DGV} cells were incubated with Nile red, the lipid marker accumulated in late endosomes, colocalizing with LBPA (not shown), but also in CDVs (Fig. 6 a). Close examination of the images revealed that the Nile red staining was within the center of the CDVs, whereas the caveolin mutant formed a characteristic ring around the vesicle (Fig. 6 a, insert and arrowheads) entirely consistent with the electron microscopic observations. The association of lipid droplets with a domain of the ER is consistent with recent studies in adipocytes (Prattes et al., 2000). As shown in Fig. 6 c, cav^{DGV} expression caused an increased intracellular accumulation of lipids compared with nontransfected cells (Fig. 6, b and c), demonstrating that cav^{DGV} expression induces a lipid storage disorder by accumulating neutral lipids inside the CDVs (arrowheads) and in other intracellular compartments (arrows). Although the intracellular accumulation of lipids induced by cav^{DGV} was variable, the mean increase in Nile red staining in cav^{DGV}-transfected cells was over twofold higher than nontransfected cells (ratio of pixels in cav^{DGV}-transfected/untransfected cells = 2.22 $\pm$ 0.89). In contrast, full-length cav-3 caused no significant accumulation of neutral lipids (ratio of cav-3-transfected/untransfected cells = 1.07 $\pm$ 0.10). Together with the electron microscopic observations, these results strongly suggest that the mutant caveolin protein specifically accumulates in the membrane of lipid droplets and that the mutant protein induces increased accumulation of neutral lipids.

Cav^{DGV} Inhibits the Post Late Endosomal Trafficking of Cholesterol and Reduces Cholesterol Efflux and Synthesis

As cav^{DGV} causes intracellular accumulation of lipids and functional studies suggest an effect on cholesterol, we next investigated the effect of cav^{DGV} expression on FC using the fluorescent cholesterol probe, filipin. In control cells, filipin labeling (which labels nonesterified FC) was found in the Golgi/recycling endosome area, on the plasma membrane, and in some scattered intracellular vesicles (Fig. 6, d and k). However, after 24–32 h of the cav^{DGV} expression a dramatic change in the filipin labeling pattern was observed: in 65% of cav^{DGV} expressing cells, there was no detectable filipin labeling on the plasma membrane (Fig. 6, arrows), in 72% of the cells, cholesterol was accumulated in very enlarged intracellular vesicles (Fig. 6, arrowheads)

identified as late endosomes for the presence of LBPA (Fig. 6, g–j) and in 90% of the cells cholesterol was not present in the perinuclear (Golgi/recycling endosome) region. Colocalization between cav^{DGV} and filipin under these conditions was rare, indicating that little FC is present in cav^{DGV} vesicles (Fig. 6, e and f, insert and k). These results suggest that cav^{DGV} promotes a similar lipid storage disorder to that occurring in lipid storage diseases in which FC accumulates in late endosomes (Kobayashi et al., 1998). To further explore this, we biochemically measured the efflux of cellular cholesterol to serum acceptors in cell cultures transfected with cav^{DGV}. COS-1 cells were transfected either with HA-tagged cav^{DGV} or vector alone and radiolabeled with [^{14}C]cholesterol as detailed in Materials and Methods. Cholesterol efflux to 20% serum during 2 h was measured 48 h after transfection. A small but significant reduction of 15% was observed in those cultures expressing cav^{DGV}, from 6.4 $\pm$ 0.14 to 5.5 $\pm$ 0.28 (% of [^{14}C]cholesterol efflux). Interestingly, although the efflux of cholesterol was reduced, the total cholesterol content of cav^{DGV} expressing cells was identical to control cells (data not shown). The level of cholesterol esterification was also not significantly modified, and the ACAT inhibitor had no effect on labeling of lipid-rich structures by the cav^{DGV} mutant (data not shown). In addition, cholesterol synthesis was reduced by $\sim$30% (from 565 $\pm$ 20 cpm/mg of protein in control cells to 384 $\pm$ 109 in cav^{DGV} cells, in three independent experiments) suggesting that this decrease may balance the decreased efflux. Taken together, we conclude that cav^{DGV} expression has a small effect on FC efflux but the major effect of the mutant protein is to induce the redistribution of cellular cholesterol pools, from the PM to late endosomes.

The decrease in plasma membrane FC and accumulation of FC in late endosomes induced by expression of DGV (24–32 h after transfection), is similar to that observed in a number of lysosomal storage diseases such as NPC1 and gangliosidoses (Kobayashi et al., 1998). This phenotype can be mimicked experimentally using the drug U18666A, a hydrophobic amine that acts on negatively charged phospholipids in the late endosomes and therefore causes late endosomal accumulation of FC (Kobayashi et al., 1998). Thus, we speculated that the drug U18666A might mimic the effect of cav^{DGV} on the cholesterol cycle. To test the synergism between cav^{DGV} expression and the U18666A drug, the cells were transfected for different times with cav^{DGV} in the presence of U18666A and the cholesterol distribution

heads and merge panel). Cells expressing cav^{DGV} showed a marked accumulation of lipids, in CDVs, and in other vesicular structures (arrows in c), compared with nontransfected cells. d–f, Cav^{DGV} HA-tagged transfected cells were labeled with filipin (to visualize cellular FC, see Materials and Methods for details) and with an mAb to the HA tag. Cav^{DGV} expression induced a marked redistribution of filipin: 65% of cav^{DGV} expressing cells did not contain filipin on the PM (arrows in d and f) and in 72% of the transfected cells filipin was detected in very enlarged cytoplasmic vesicles (arrowheads and insert f). g–j, Cav^{DGV} HA-tagged transfected cells were labeled with filipin (blue) and with antibodies to the HA tag (red) and to LBPA (green). Cav^{DGV} expression induced redistribution of FC to very enlarged late endosomes (arrows in i and j). k–m, BHK were transfected with cav^{DGV} in a normal medium (k) or in a medium containing 4.5 μg/ml of U18666A (l and m) for different times and cholesterol distribution was monitored by means of filipin. In cells expressing cav^{DGV}, a complete accumulation of lipids in late endosomes was evident after 24–32 h (k). However, in those cells expressing cav^{DGV} in the presence of U18666A the complete accumulation of FC in late endosomes was evident after 16 h (l), demonstrating that the combination of the drug and the cav^{DGV} results in an earlier lysosomal storage disorder. Finally, after 24 h few differences could be observed between nonexpressing and cav^{DGV} expressing cells, but some very enlarged intracellular vesicles were present in transfected cells (arrows in m). Bar, 5 μm.
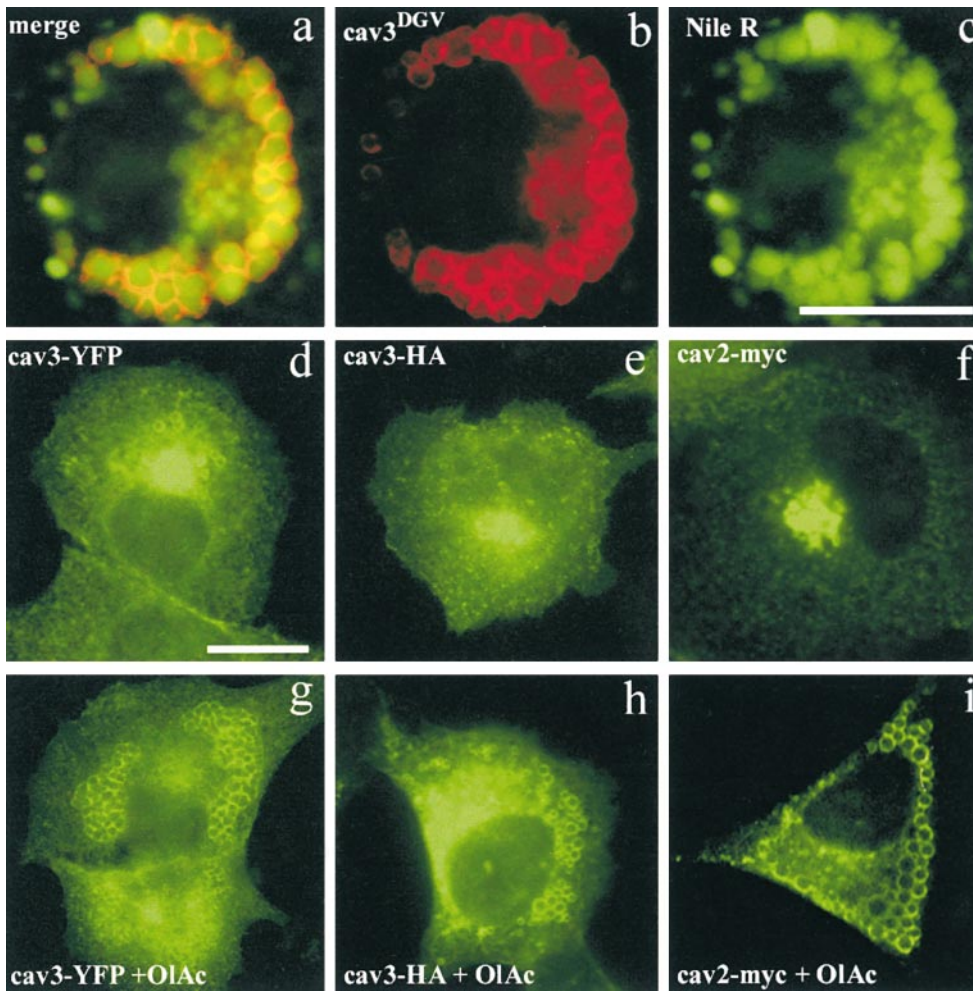
Figure 7. Full-length caveolins and cav^DGV accumulate on lipid droplets formed in response to oleic acid treatment. a–c, BHK cells preincubated in a medium containing oleic acid for 16 h, were transfected with HA-tagged cav^DGV, incubated for an additional 24 h in a medium containing oleic acid, labeled with antibodies to HA tag and finally mounted in mowiol containing Nile red (see Materials and Methods for details). Cav^DGV (b) was exclusively detected surrounding very enlarged Nile red-positive lipid droplets (c). d–i, Untreated BHK (d, e, and f) or cells preincubated in a medium containing oleic acid for 16 h (g, h, and i) were transfected with YFP-tagged cav-3 (d and g), HA-tagged cav-3 (e and h), or myc-tagged cav-2 (f and i) and incubated for an additional 24 h in medium with or without oleic acid. Cells transfected with HA or myc tag were labeled with specific antibodies and cells transfected with the YFP-tagged constructs were mounted without any additional manipulation after fixation. 65% of cells transfected with cav-3-YFP showed, in addition to PM and Golgi complex usual labeling, some intracellular rings (d). In contrast, very few rings were observed in those cells transfected with HA-cav-3 (e). After oleic acid treatment, in 98% of the cells transfected with YFP-tagged (g) or 52% of the cells transfected with HA-tagged cav-3 (h) the protein, in addition to the PM labeling, was observed on lipid droplets (Nile red staining not shown). Myc-tagged cav-2 showed a dramatic redistribution from the Golgi area in control cells (f) to the lipid droplets after oleic acid treatment (i). Bars, 5 μm.

was monitored by means of filipin. In cells expressing cav^DGV, a complete accumulation of lipids in late endosomes was evident after just 16 h of the transfection and U18666A treatment (Fig. 6 l) demonstrating that the combination of the drug and the mutant results in an earlier lysosomal storage disorder. After 24 h, the intracellular accumulation of filipin in nontransfected cells resembled cav^DGV expressing cells, but some characteristic enlarged vesicles could be observed in transfected cells (Fig. 6 m, arrow). These results show that U18666A causes the accumulation of FC in late endosomes in a synergistic manner with the cav^DGV mutant, suggesting that both treatments affect different steps of the same transport pathway.

Full-length Caveolins and cav^DGV Accumulate on Lipid Droplets Formed in Response to Oleic Acid Treatment

To further investigate the association of full-length caveolins with bona fide lipid droplets, cells were treated with oleic acid (Brasaemle et al., 1997) to induce lipid droplet accumulation. Untreated cells transfected with full-length cav-3 HA showed some colocalization with Nile red, but

few large rings (only 10% of the cells contained evident rings; Fig. 7 e). In contrast, 65% of cells transfected with cav-3 YFP showed intracellular rings (Fig. 7 d). Cells were then treated with oleic acid, which caused increased accumulation of enlarged Nile red positive lipid droplets (see example in Fig. 7 c). As expected, cav^DGV was exclusively detected surrounding the enlarged droplets (Fig. 7 a). In addition, full-length cav-3 was now associated with the droplets in the majority of oleic acid-treated cells (98% of the cells transfected with YFP-tagged cav-3; 52% of cells with HA-tagged cav-3), as well as showing plasma membrane and Golgi complex labeling. Full-length VSVG-tagged cav-1 distributed in a similar manner to HA-tagged cav-3, although the accumulation on lipid droplets was less evident. However, endogenous cav-1 was rarely observed on rings even after the oleic acid treatment, although in some cells (10%) it was observed in a very dotted and weak pattern around some of the droplets (not shown). In contrast, myc-tagged cav-2 showed a dramatic and complete redistribution from the Golgi area in control cells (Fig. 7 f) to the lipid droplets after oleic acid treatment (Fig. 7 i).

Discussion

Caveolin Mutants and Wild-type Caveolins Access Lipid-containing Bodies

In the present study, we have shown that a caveolin mutant, which disrupts specific signaling pathways, induces a cholesterol trafficking defect in the expressing cells. The cav^{DGV} containing compartment (CDV) shows the characteristics of lipid droplets, being large, nonacidic, spherical structures that are labeled by the neutral lipid dye, Nile red. We have shown by electron microscopy with three different techniques that a membrane surrounds the lipid droplets and that this membrane contains the caveolin mutant protein that behaves as an integral membrane protein biochemically. Morphologically identical structures are observed in nontransfected cells suggesting that they are not generated exclusively by expression of the mutant protein. However, staining with a neutral lipid dye strongly suggests that they are enlarged in the mutant-expressing cells. The localization of a caveolin mutant to a lipid droplet associated with the ER implicates caveolin in lipid transport to/from lipid droplets. The mutant may be accumulating aberrantly in a transient station on the caveolin cycling pathway. This hypothesis is supported by the fact that cav-3^{DGV} and fluorescent-tagged full-length caveolins are efficiently targeted to enlarged lipid droplets induced by oleic acid treatment. Importantly, these experiments also demonstrate that cav^{DGV} accumulates specifically on preexisting lipid droplets rather than only inducing the formation of new structures. Our studies also show that expressed and epitope-tagged wild-type caveolins, although predominantly associated with the plasma membrane and Golgi complex, can also associate with lipid droplets. Cav-2 showed a particular propensity for lipid droplets as shown in oleic acid-treated cells. Further work will be required to ascertain whether the ready visualization of the tagged proteins in the lipid droplets, as compared with the endogenous proteins, may simply reflect the higher levels of the expressed proteins or the inaccessibility of caveolin epitopes in specific compartments (Luetterforst et al., 1999). Importantly, coimmunoprecipitation experiments with antibodies to the epitope-tagged cav^{DGV} mutant show that the mutant protein associates with both endogenous cav-1 and cav-2 (not shown).

Molecular Requirements for Targeting to CDVs

Our results suggest that the absence of the NH$_2$ terminus of caveolin causes association with lipid droplets and possibly disruption of exit from the ER. The localization of the DGV mutants (cav-3^{DGV}, cav-1^{DGI}, and cav-2^{DKV}) is quite distinct from a shorter truncation mutant, cav-3^{NED} (residues from 33 to 151; see Luetterforst et al., 1999) or cav-1$_{60-178}$ described recently as the equivalent truncation of cav-3^{DGV} for cav-1. Notice that since cav-1 is 27 residues longer at the NH$_2$ terminus than cav-3 (178 aa and 151 aa respectively), the equivalent truncation for cav-3^{DGV} in cav-1 is the deletion of 81 residues of the NH$_2$-terminal domain up to the scaffolding domain, referred as cav-1^{DGI} in this paper (Machleidt et al., 2000). The cav^{DGV} mutants do not label the plasma membrane and accumulate in the CDVs, whereas cav^{NED} labels the Golgi complex and cell

surface in a similar manner to the wild-type protein or the cav-1$_{60-178}$. This suggests that the region between residues 33 and 53 is of critical importance in attaining its steady state distribution and perhaps in exit from the CDVs/ER lipid droplets. The inability to move out of this compartment may lead to the phenotypic changes described here. The 21 residues sequence (NEDIVKVDFEDVIAEPEGTYS) shows very high homology to the same region of cav-1 and cav-2 and the nine central residues are almost identical in all three caveolin members. Because all three caveolin members can access the DGV compartment, it will be of great interest to ascertain whether specific proteins can bind to cav^{NED}, but not cav^{DGV}. In addition, because this region mediates the oligomerization of caveolins (Sargiacomo et al., 1995) it will be important to elucidate if oligomerization is necessary for the exit from the ER. The conserved scaffolding domain of caveolin is not necessary for targeting caveolins to CDVs as the cav^{LLS} mutant (residues from 75 to 151) shows a similar accumulation to cav^{DGV} (this study) and also is a potent and specific inhibitor of H-ras mediated Raf activation (Pol, A., and R.G. Parton, manuscript in preparation) presumably by a similar mechanism to cav^{DGV} (Roy et al., 1999).

The Caveolin Cycle and Cholesterol Balance

Expression of the cav^{DGV} mutant causes increased intracellular accumulation of FC and a decrease in plasma membrane FC as judged by filipin staining. This is consistent with previous studies showing that expression of cav^{DGV} inhibits Raf-mediated H-Ras activation and that this inhibition could be mimicked by cholesterol depletion and rescued by cholesterol readdition (Roy et al., 1999). A striking effect of cav^{DGV} is the accumulation of FC intracellularly within enlarged late endosomes and therefore the phenotype of the mutant-expressing cells appears similar to the well-characterized phenotype of NPC1−/− cells. Consistent with this hypothesis, a recent study suggested that NPC1−/− neurons are unable to respond to the neurotrophin, BDNF (Henderson et al., 2000). The link between the cav^{DGV} phenotype and cholesterol disorders is further strengthened by the finding that the drug U18666A mimics the NPC1−/− and the DGV phenotype causing the accumulation of FC in late endosomes. U18666A is thought to act at the level of the late endosomes/lysosomes to alter the flow of cholesterol between internal pools and recent evidence suggests that the NPC1 protein and U18666A work in a similar transport step (Lange et al., 2000). In contrast to the phenotype of NPC1−/− fibroblasts, the cav^{DGV} mutant had no effect on cholesterol esterification but did cause a small decrease in both cholesterol efflux and cholesterol biosynthesis. The net result of these changes was that there was no major change in total cellular cholesterol levels in the cav^{DGV}-expressing cells.

In conclusion, our studies raise the possibility that caveolin play a role in trafficking of lipids to/from lipid droplets. Whether caveolin cycles through this compartment under physiological conditions requires further investigation, but our studies suggest that lipid droplet formation in response to oleic acid and cholesterol manipulation causes wild-type caveolin to accumulate in these structures (Pol, A., and R.G. Parton, unpublished information). The stud-

ies presented here identify the underlying defect in cells expressing a caveolin dominant negative mutant as a lipid transport defect and strongly implicate caveolins in lipid transport. They also provide new tools to dissect the crucial role of lipid transport in diverse cellular processes and to understand the role of caveolins in cell physiology.

References

Babitt, J., B. Trigatti, A. Rigotti, E.J. Smart, R.G. Anderson, S. Xu, and M. Krieger. 1997. Murine SR-BI, a high density lipoprotein receptor that mediates selective lipid uptake, is N-glycosylated and fatty acylated and colocalizes with plasma membrane caveolae. *J. Biol. Chem.* 272:13242–13249.

Bist, A., P.E. Fielding, and C.J. Fielding. 1997. Two sterol regulatory element-like sequences mediate up-regulation of caveolin gene transcription in response to low density lipoprotein free cholesterol. *Proc. Natl. Acad. Sci. USA.* 94:10693–10698.

Brasaemle, D.L., T. Barber, A.R. Kimmel, and C. Londos. 1997. Post-translational regulation of perilipin expression. Stabilization by stored intracellular neutral lipids. *J. Biol. Chem.* 272:9378–9387.

Brown, M.S., and J.L. Goldstein. 1997. The SREBP pathway: regulation of cholesterol metabolism by proteolysis of a membrane-bound transcription factor. *Cell.* 89:331–340.

Carozzi, A.J., E. Ikonen, M.R. Lindsay, and R.G. Parton. 2000. Role of cholesterol in developing T-Tubules: analogous mechanisms for T-Tubules formation and caveolae biogenesis. *Traffic.* 1:326–341.

Dupree, P., R.G. Parton, G. Raposo, T.V. Kurzchalia, and K. Simons. 1993. Caveolae and sorting in the trans-Golgi network of epithelial cells. *EMBO (Eur. Mol. Biol. Organ.) J.* 12:1597–1605.

Fielding, C.J., and P.E. Fielding. 1997. Intracellular cholesterol transport. *J. Lipid Res.* 38:1503–1521.

Gagescu, R., N. Demaurex, R.G. Parton, W. Hunziker, L.A. Huber, and J. Gruenberg. 2000. The recycling endosome of Madin-Darby canine kidney cells is a mildly acidic compartment rich in raft components. *Mol. Biol. Cell.* 11:2775–2791.

Garver, W.S., R.P. Erickson, J.M. Wilson, T.L. Colton, G.S. Hossain, M.A. Kozloski, and R.A. Heidenreich. 1997. Altered expression of caveolin-1 and increased cholesterol in detergent insoluble membrane fractions from liver in mice with Niemann-Pick disease type C. *Biochim. Biophys. Acta.* 1361:272–280.

Garver, W.S., R.A. Heidenreich, R.P. Erickson, M.A. Thomas, and J.M. Wilson. 2000. Localization of the murine Niemann-Pick C1 protein to two distinct intracellular compartments. *J. Lipid Res.* 41:673–687.

Griffiths, G., M. Ericsson, J. Krijnse-Locker, T. Nilsson, B. Goud, H.D. Soling, B.L. Tang, S.H. Wong, and W. Hong. 1994. Localization of the Lys, Asp, Glu, Leu tetrapeptide receptor to the Golgi complex and the intermediate compartment in mammalian cells. *J. Cell Biol.* 127:1557–1574.

Heino, S., S. Lusa, P. Somerharju, C. Ehnholm, V.M. Olkkonen, and E. Ikonen. 2000. Dissecting the role of the Golgi complex and lipid rafts in biosynthetic transport of cholesterol to the cell surface. *Proc. Natl. Acad. Sci. USA.* 97: 8375–8380.

Henderson, L.P., L. Lin, A. Prasad, C.A. Paul, T.Y. Chang, and R.A. Maue. 2000. Embryonic striatal neurons from niemann-pick type C mice exhibit defects in cholesterol metabolism and neurotrophin responsiveness. *J. Biol. Chem.* 275:20179–20187.

Hua, X., A. Nohturfft, J.L. Goldstein, and M.S. Brown. 1996. Sterol resistance in CHO cells traced to point mutation in SREBP cleavage-activating protein. *Cell.* 87:415–426.

Kaplan, M.R., and R.D. Simoni. 1985. Transport of cholesterol from the endoplasmic reticulum to the plasma membrane. *J. Cell Biol.* 101:446–453.

Kobayashi, T., E. Stang, K.S. Fang, P. de Moerloose, R.G. Parton, and J. Gruenberg. 1998. A lipid associated with the antiphospholipid syndrome regulates endosome structure and function. *Nature.* 392:193–197.

Kurzchalia, T.V., and R.G. Parton. 1999. Membrane microdomains and caveolae. *Curr. Opin. Cell Biol.* 11:424–431.

Kurzchalia, T.V., P. Dupree, R.G. Parton, R. Kellner, H. Virta, M. Lehnert, and K. Simons. 1992. VIP21, a 21-kD membrane protein is an integral component of trans-Golgi-network-derived transport vesicles. *J. Cell Biol.* 118: 1003–1014.

Lange, Y., J. Ye, M. Rigney, and T. Steck. 2000. Cholesterol movement in Niemann-Pick type C cells and in cells treated with amphiphiles. *J. Biol. Chem.* 275:17468–17475.

Liu, P., W.P. Li, T. Machleidt, and R.G. Anderson. 1999. Identification of caveolin-1 in lipoprotein particles secreted by exocrine cells. *Nat. Cell Biol.* 1:369–375.

Liscum, L. 2000. Niemann-Pick type C mutations cause lipid traffic jam. *Traffic.* 1:218–225.

Luetterforst, R., E. Stang, N. Zorzi, A. Carozzi, M. Way, and R.G. Parton. 1999. Molecular characterization of caveolin association with the Golgi complex: identification of a cis-Golgi targeting domain in the caveolin molecule. *J. Cell Biol.* 145:1443–1459.

Machleidt, T., W.P. Li, P. Liu, and R.G. Anderson. 2000. Multiple domains in caveolin-1 control its intracellular traffic. *J. Cell Biol.* 148:17–28.

Marigo, V., R.A. Davey, Y. Zuo, J.M. Cunningham, and C.J. Tabin. 1996. Biochemical evidence that patched is the Hedgehog receptor. *Nature.* 384:176–179.

Mayor, S., S. Sabharanjak, and F.R. Maxfield. 1998. Cholesterol-dependent retention of GPI-anchored proteins in endosomes. *EMBO (Eur. Mol. Biol. Organ.) J.* 17:4626–4638.

Murata, M., J. Peranen, R. Schreiner, F. Wieland, T.V. Kurzchalia, and K. Simons. 1995. VIP21/caveolin is a cholesterol-binding protein. *Proc. Natl. Acad. Sci. USA.* 92:10339–10343.

Parton, R.G. 1994. Ultrastructural localization of gangliosides: GM1 is concentrated in caveolae. *J. Histochem. Cytochem* 42:155–166.

Pol, A., M. Calvo, A. Lu, and C. Enrich. 1999. The "early-sorting" endocytic compartment of rat hepatocytes is involved in the intracellular pathway of caveolin-1 (VIP-21). *Hepatology.* 29:1848–1857.

Porter, J.A., K.E. Young, and P.A. Beachy. 1996. Cholesterol modification of hedgehog signaling proteins in animal development [published erratum appears in *Science.* 1996. 274:1597]. *Science.* 274:255–259.

Prattes, S., G. Horl, A. Hammer, A. Blaschitz, W.F. Graier, W. Sattler, R. Zechner, and E. Steyrer. 2000. Intracellular distribution and mobilization of unesterified cholesterol in adipocytes: triglyceride droplets are surrounded by cholesterol-rich ER-like surface layer structures. *J. Cell Sci.* 113:2977–2989.

Rojo, M., R. Pepperkok, G. Emery, R. Kellner, E. Stang, R.G. Parton, and J. Gruenberg. 1997. Involvement of the transmembrane protein p23 in biosynthetic protein transport. *J. Cell Biol.* 139:1119–1135.

Roy, S., R. Luetterforst, A. Harding, A. Apolloni, M. Etheridge, E. Stang, B. Rolls, J.F. Hancock, and R.G. Parton. 1999. Dominant-negative caveolin inhibits H-Ras function by disrupting cholesterol-rich plasma membrane domains. *Nat. Cell Biol.* 1:98–105.

Sargiacomo, M., P.E. Scherer, Z. Tang, E. Kubler, K.S. Song, M.C. Sanders, and M.P. Lisanti. 1995. Oligomeric structure of caveolin: implications for caveolae membrane organization. *Proc. Natl. Acad. Sci. USA.* 92:9407–9411.

Scheiffele, P., P. Verkade, A.M. Fra, H. Virta, K. Simons, and E. Ikonen. 1998. Caveolin-1 and -2 in the exocytic pathway of MDCK cells. *J. Cell Biol.* 140: 795–806.

Smart, E.J., Y.S. Ying, P.A. Conrad, and R.G. Anderson. 1994. Caveolin moves from caveolae to the Golgi apparatus in response to cholesterol oxidation. *J. Cell Biol.* 127:1185–1197.

Smart, E.J., Y. Ying, W.C. Donzell, and R.G. Anderson. 1996. A role for caveolin in transport of cholesterol from endoplasmic reticulum to plasma membrane. *J. Biol. Chem.* 271:29427–29435.

Spillane, D.M., J.W. Reagan, Jr., N.J. Kennedy, D.L. Schneider, and T.Y. Chang. 1995. Translocation of both lysosomal LDL-derived cholesterol and plasma membrane cholesterol to the endoplasmic reticulum for esterification may require common cellular factors involved in cholesterol egress from the acidic compartments (lysosomes/endosomes). *Biochim. Biophys. Acta.* 1254:283–294.

Trigatti, B.L., R.G. Anderson, and G.E. Gerber. 1999. Identification of caveolin-1 as a fatty acid binding protein. *Biochem. Biophys. Res. Commun.* 255: 34–39.

Uittenbogaard, A., and E.J. Smart. 2000. Palmitoylation of caveolin-1 is required for cholesterol binding, chaperone complex formation, and rapid transport of cholesterol to caveolae. *J. Biol. Chem.* 275:25595–25599.

Uittenbogaard, A., Y. Ying, and E.J. Smart. 1998. Characterization of a cytosolic heat-shock protein-caveolin chaperone complex. Involvement in cholesterol trafficking. *J. Biol. Chem.* 273:6525–6532.

Underwood, K.W., N.L. Jacobs, A. Howley, and L. Liscum. 1998. Evidence for a cholesterol transport pathway from lysosomes to endoplasmic reticulum that is independent of the plasma membrane. *J. Biol. Chem.* 273:4266–4274.

Urbani, L., and R.D. Simoni. 1990. Cholesterol and vesicular stomatis virus G protein take separate routes from the endoplasmic reticulum to the plasma membrane. *J. Biol. Chem.* 265:1919–1923.

van Genderen, I.L., G. van Meer, J.W. Slot, H.J. Geuze, and W.F. Voorhout. 1991. Subcellular localization of Forssman glycolipid in epithelial MDCK cells by immuno-electronmicroscopy after freeze-substitution. *J. Cell Biol.* 115:1009–1019.

Voorhout, W.F., T. Veenendaal, H.P. Haagsman, A.J. Verkleij, L.M. van Golde, and H.J. Geuze. 1991. Surfactant protein A is localized at the corners of the pulmonary tubular myelin lattice. *J. Histochem. Cytochem.* 39:1331–1336.